Models for the polarized parton distributions of the nucleon

M. Glück,[1] E. Reya,[1] M. Stratmann,[2] and W. Vogelsang[3]

[1]*Universität Dortmund, Institut für Physik, D-44221 Dortmund, Germany*
[2]*Institut für Theoretische Physik, Universität Regensburg, D-93040 Regensburg, Germany*
[3]*RIKEN-BNL Research Center, Brookhaven National Laboratory, Upton, New York 11973*

Polarized deep inelastic scattering (DIS) data are analyzed in leading and next-to-leading order of QCD within the common ''standard'' scenario of polarized parton distributions with a flavor-symmetric light sea (antiquark) distribution $\delta\bar{q}$, and a completely $SU(3)_f$ broken ''valence'' scenario with totally flavor-asymmetric light sea densities ($\delta\bar{u} \neq \delta\bar{d} \neq \delta\bar{s}$). The latter flavor-broken light sea distributions are modeled with the help of a Pauli-blocking ansatz at the low radiative or dynamical input scales of $\mu^2_{\text{LO(NLO)}} = 0.26$ (0.40) GeV^2 which complies with predictions of the chiral quark-soliton model and expectations based on the statistical parton model as well as with the corresponding, well established, flavor-broken unpolarized sea ($\bar{d} > \bar{u}$). Present semi-inclusive DIS data cannot yet uniquely discriminate between those two flavor-symmetric and flavor-broken polarized light sea scenarios.

I. INTRODUCTION

The polarized parton distributions of the nucleon have been intensively studied in recent years [1–14]. The conclusion has been that the experimental data dictate a negatively polarized antiquark component, and show a tendency toward a positive polarization of gluons. Presently we possess a lot of precise data [15–24] on the polarized structure functions of the nucleon, some of them very recent [23,24], which justify a renewed investigation of the aforementioned issue. This alone, however, does not provide the main motivation for this project, rather the improved understanding in recent years of the situation in the *unpolarized* parton sector [25–28] provides important insights for the corresponding *polarized* parton densities. In particular, one notes that the unpolarized sea (antiquark) distributions are flavor asymmetric ($\bar{d} > \bar{u}$), which can be understood in terms of flavor mass asymmetries and Pauli-blocking effects [29,30]. The main objective of the present paper is to transcribe these insights into the polarized parton sector as will be described in Sec. III. In Sec. II we shall, for completeness, present an analysis within the framework of the simplified $SU(3)_f$ symmetric ''standard'' scenario in which the flavor asymmetries in the polarized antiquark sector are neglected. This is done in view of the fact that in many situations these flavor asymmetries are unobservable as is the case for (most) presently available data which cannot provide any reliable information concerning this issue.

Measurements of polarized deep-inelastic lepton nucleon scattering yield direct information [15–24] on the spin asymmetry

$$A_1^N(x,Q^2) \simeq \frac{g_1^N(x,Q^2)}{F_1^N(x,Q^2)} = \frac{g_1^N(x,Q^2)}{F_2^N(x,Q^2)/\{2x[1+R^N(x,Q^2)]\}},$$
$$(1.1)$$

$N = p$, n and $d = (p+n)/2$ where in the latter case we have used $g_1^d = (g_1^p + g_1^n)[1 - 3\omega_D/2]/2$ with $\omega_D = 0.058$, R

$\equiv F_L/2xF_1 = (F_2 - 2xF_1)/2xF_1$ and subdominant contributions have, as usual, been neglected.

We emphasize that, as in our original analysis [1], we compute *both* g_1 and F_1 entirely in leading-twist QCD. In particular, in order to obtain F_1, we use the parton densities of Glück, Reya, and Vogt (GRV98) [25] along with leading order (LO) (note that $R = 0$ at leading order) or next-to-LO (NLO) coefficient functions for F_2 and R in Eq. (1.1). An alternative, frequently adopted [3,4,5,9,10,13] approach is to take $F_2(x,Q^2)$ and $R(x,Q^2)$ from experimental measurements, which is motivated by the fact that leading-twist calculations of $F_2(x,Q^2)$ and $R(x,Q^2)$ do not agree very well with experimental determinations in the region of low Q^2 and $W^2 = Q^2(1-x)/x$. These regions are affected by power-suppressed contributions and are therefore excluded from all unpolarized deep inelastic scattering (DIS) analyses. The presently available data in the polarized case, however, do not allow to impose similarly ''safe'' cuts ($Q^2 \geq 4$ GeV^2, $W^2 \geq 10$ GeV^2) without losing too much information. On the other hand, the Q^2 range accessed so far in polarized DIS does not allow for extracting the magnitude and shape of power-suppressed contributions reliably. To study the issue further, we performed fits to the A_1 data in both possible ways, i.e., with leading-twist calculations of F_2 and R *as well* as with their experimental results, admitting at the same time an ''effective higher-twist'' contribution to A_1 in terms of a factor $[1 + A(x)/Q^2]$ with $A(x)$ to be determined by the data. The outcome of this analysis was that $A(x)$ is consistent with zero if we use leading-twist QCD for F_2 and R, but that it is sizeable and important in the fit if F_2 and R are taken from experiment. We take this as an indication that our preferred approach is more consistent and less liable to modifications by higher-twist terms. This view is also corroborated by the fact that the deep inelastic scattering (DIS) A_1 data show only a very mild Q^2 dependence, even toward low values of Q^2. The consistency of the polarized parton densities as extracted from DIS data at comparatively low values of Q^2 with measurements of other hard processes at

63 094005-1

higher scales can be studied soon at RHIC and perhaps in the future at a polarized ep collider.

In NLO, $g_1^N(x,Q^2)$ is related to the polarized (anti)quark and gluon distributions $\delta f(x,Q^2) \equiv f_+ - f_-$ in the following way:

$$g_1^N(x,Q^2) = \frac{1}{2} \sum_q e_q^2 \left[\delta q^N(x,Q^2) + \delta \bar{q}^N(x,Q^2) \right.$$
$$\left. + \frac{\alpha_s(Q^2)}{2\pi} \left(\delta C_q * (\delta q^N + \delta \bar{q}^N) + \frac{1}{f} \delta C_g * \delta g \right) \right]$$
(1.2)

with the convolutions $\delta C_f * f$ being defined in the usual way. The modified minimal subtraction scheme ($\overline{\text{MS}}$) coefficient functions $\delta C_f(x)$ can be also found in Ref. [1], where all necessary ingredients for the Q^2 evolution have been formulated as well. A similar expression holds for the unpolarized structure function $F_1^N(x,Q^2)$ with its spin-averaged parton distributions $f(x,Q^2) \equiv f_+ + f_-$ and the unpolarized Wilson coefficients can be found, for example, in Ref. [31]. The LO and NLO ($\overline{\text{MS}}$) input scales, running coupling constants and parton distributions, employed in the positivity constraints $|\delta f| \leq f$, will be adopted from GRV98 [25]. Furthermore we shall, as always, use the notation $\delta q^p \equiv \delta q$ and $q^p \equiv q$, and neglect the marginal charm contribution to g_1^N stemming from the subprocess $\vec{\gamma} * \vec{g} \to c \bar{c}$ [32]. The charm contribution to F_1^N is also small in the kinematic range covered by present polarization experiments.

The total helicity of a specific parton $f = u, \bar{u}, d, \bar{d}, s, \bar{s}, g$ is given by the first ($n=1$) moment

$$\Delta f(Q^2) \equiv \int_0^1 dx\, \delta f(x,Q^2).$$
(1.3)

Thus, according to Eq. (1.2),

$$\Gamma_1(Q^2) \equiv \int_0^1 dx\, g_1(x,Q^2) = \frac{1}{2} \sum_q e_q^2 [\Delta q(Q^2) + \Delta \bar{q}(Q^2)]$$
$$\times \left(1 - \frac{\alpha_s(Q^2)}{\pi} \right)$$
(1.4)

since $\Delta C_q = -3C_F/2 = -2$ and $\Delta C_g = 0$. Therefore we have in general

$$\Gamma_1^{p,n}(Q^2) = \left[\pm \frac{1}{12} \Delta q_3 + \frac{1}{36} \Delta q_8 + \frac{1}{9} \Delta \Sigma(Q^2) \right] \left(1 - \frac{\alpha_s(Q^2)}{\pi} \right)$$
(1.5)

with the flavor-nonsinglet components

$$\Delta q_3 \equiv \Delta u + \Delta \bar{u} - \Delta d - \Delta \bar{d},$$
(1.6)

$$\Delta q_8 \equiv \Delta u + \Delta \bar{u} + \Delta d + \Delta \bar{d} - 2(\Delta s + \Delta \bar{s})$$
(1.7)

being conserved, i.e., Q^2 independent, and the flavor-singlet component is given by

$$\Delta \Sigma(Q^2) \equiv \sum_{q=u,d,s} [\Delta q(Q^2) + \Delta \bar{q}(Q^2)] = \Delta q_8 + 3[\Delta s(Q^2)$$
$$+ \Delta \bar{s}(Q^2)].$$
(1.8)

These quantities will be subject to various constraints (derived from hyperon β decays) depending on the specific model scenarios under consideration to which we shall turn in the next two sections.

Finally, the fundamental helicity sum rule reads

$$\frac{1}{2} = \frac{1}{2} \Delta \Sigma(Q^2) + \Delta g(Q^2) + L_{q+g}(Q^2),$$
(1.9)

where L_{q+g} refers to the total orbital contribution of all (anti)quarks and gluons to the spin of the proton.

II. SU(3)$_f$ SYMMETRIC "STANDARD" (UNBROKEN-SEA) SCENARIO

As stated in the Introduction, present data do not provide sufficient information concerning the flavor asymmetries of the polarized sea distributions. Thus present day studies must, as a first approximation, neglect this issue unless one is willing to adopt some models for the flavor asymmetries as will be done in Sec. III. Here we follow the procedure presented by Glück, Reya, Stratmann, and Vogelsang (GRSV95) [1]. The searched for polarized NLO (as well as LO) parton distributions $\delta f(x,Q^2)$, compatible with present data [15–24] on $A_1^N(x,Q^2)$, are constrained by the standard sum rules

$$\Delta q_3 = F + D = g_A = 1.2670 \ (35), \quad (2.1)$$

$$\Delta q_8 = 3F - D = 0.58 \pm 0.15, \quad (2.2)$$

where the updated values for F and D have been taken into account [33] and the error estimate in Eq. (2.2) is due to Ref. [34]. Thus Eq. (1.5) becomes

$$\Gamma_1^{p,n}(Q^2) = \left[\pm \frac{1}{12}(F+D) + \frac{5}{36}(3F-D) + \frac{1}{3}[\Delta s(Q^2) + \Delta \bar{s}(Q^2)] \right] \left(1 - \frac{\alpha_s(Q^2)}{\pi} \right),$$
(2.3)

i.e., one needs here a finite sizeable strange sea polarization $\Delta s(Q^2) < 0$ in order to achieve the experimentally required reduction of the Ellis-Jaffe LO expectation [35]

$$\Gamma_{1,\text{EJ}}^p = \frac{1}{12}(F+D) + \frac{5}{36}(3F-D) \approx 0.186.$$
(2.4)

Furthermore, in the standard scenario one assumes an unbroken SU(3)$_f$ symmetric sea,

$$\delta \bar{q}(x,Q^2) \equiv \delta \bar{u} = \delta u_{\text{sea}} = \delta \bar{d} = \delta d_{\text{sea}} = \delta s = \delta \bar{s}. \quad (2.5)$$

For the determination of the NLO (LO) polarized parton distributions $\delta f(x,Q^2)$ we follow our original analysis [1] by relating the polarized input densities to the unpolarized ones,

TABLE I. The parameters of the LO and NLO input parton distributions, as defined in Eq. (2.6), at $\mu_{LO}^2 = 0.26$ GeV^2 and $\mu_{NLO}^2 = 0.40$ GeV^2, respectively, for the standard scenario as obtained from fits to the data in Refs. [15–24].

	Standard scenario	
	LO	NLO
N_u	0.851	1.019
α_u	0.45	0.52
β_u	0	0.12
N_d	−0.734	−0.669
α_d	0.49	0.43
β_d	0.03	0
$N_{\bar{q}}$	−0.587	−0.272
$\alpha_{\bar{q}}$	0.68	0.38
$\beta_{\bar{q}}$	0	0
N_s	1	1
N_g	1.669	1.419
α_g	1.79	1.43
β_g	0.15	0.15
χ^2/209 data pts.	174.9	169.8

using some intuitive theoretical arguments [36] as guidelines. We employ the following ansatz for the LO and NLO($\overline{\text{MS}}$) polarized parton distributions at an input scale $Q^2 = \mu^2$ [37]:

$$\delta u(x,\mu^2) = N_u x^{\alpha_u}(1-x)^{\beta_u} u(x,\mu^2)_{\text{GRV}},$$

$$\delta d(x,\mu^2) = N_d x^{\alpha_d}(1-x)^{\beta_d} d(x,\mu^2)_{\text{GRV}},$$

$$\delta \bar{q}(x,\mu^2) = N_{\bar{q}} x^{\alpha_{\bar{q}}}(1-x)^{\beta_{\bar{q}}} \bar{q}(x,\mu^2)_{\text{GRV}},$$

$$\delta g(x,\mu^2) = N_g x^{\alpha_g}(1-x)^{\beta_g} g(x,\mu^2)_{\text{GRV}}, \quad (2.6)$$

with the LO and NLO unpolarized input densities referring to the ones of GRV98 [25] and $\bar{q} \equiv (\bar{u} + \bar{d})/2$ should be considered as the reference light sea distribution for the standard unbroken-sea scenario in Eq. (2.5). The parameters of our optimal LO densities at $\mu_{LO}^2 = 0.26$ GeV^2 and the ones of the NLO($\overline{\text{MS}}$) densities at $\mu_{NLO}^2 = 0.40$ GeV^2 are given in Table I. These optimal LO and NLO($\overline{\text{MS}}$) fits correspond to a χ^2 per degree of freedom (χ_{DF}^2) of $\chi_{DF,LO}^2 = 0.84$ and to $\chi_{DF,NLO}^2 = 0.81$. The polarized gluon density in Eq. (2.6) is, as usual, rather weakly constrained by present data. Although a fully saturated (via the positivity constraint) gluon input $\delta g(x,\mu^2) = \pm g(x,\mu^2)$ is disfavored, a less saturated $\delta g(x,\mu^2) = \pm xg(x,\mu^2)$ input or even a vanishing (purely dynamical) input $\delta g(x,\mu^2) = 0$ are fully compatible with present data. The latter choice, however, seems to be unlikely in view of $\delta \bar{q}(x,\mu^2) \neq 0$.

In Fig. 1 our NLO results are compared with the data on $A_1^N(x,Q^2)$ as well as with our old original NLO($\overline{\text{MS}}$) fit [1].

The differences between these two results are small, except perhaps for A_1^n in the large-x region. Our new LO fit is similar to the NLO one shown in Fig. 1 by the solid curves. The Q^2 dependence of our LO and NLO standard scenario fits at various fixed values of x is shown in Fig. 2 and compared with all recent data on $g_1^p(x,Q^2)$, including the most recent E155 proton data [24]. The main reason for our LO results being larger than the NLO ones in the small-x region is due to the vanishing of $R^p(x,Q^2)$ in LO in Eq. (1.1). The corresponding x dependence of $g_1^N(x,Q^2 = 5$ GeV$^2)$ is shown in NLO in Fig. 3 where the expected extrapolations into the yet unmeasured small-x region down to $x = 10^{-3}$ are shown as well. The solid curves refer to our optimal NLO fit (with the input given in Table I) and allowing our optimal total χ^2 in Table I to vary by one unit, $\delta\chi^2 = \pm 1$, gives rise to the shaded areas due to different choices of the polarized gluon input at $Q^2 = \mu_{NLO}^2$ in Eq. (2.6) such as $\delta g = \pm xg$, etc. In particular, a vanishing polarized gluon input $\delta g(x,\mu_{NLO}^2) = 0$, is for the time being entirely compatible with all present data as shown by the dashed curves. On the other hand, fully saturated (via the positivity constraint) gluon inputs $\delta g(x,\mu_{NLO}^2) = \pm g$ appear to be disfavored by present data as shown by the dotted curves in Fig. 3. It should be furthermore noted that the shaded bands in Fig. 3 contain polarized gluon densities which correspond to first moments $\Delta g(Q^2 = 5$ GeV$^2)$ between −0.81 and 1.73, according to input moments between $\Delta g(\mu_{NLO}^2) = -0.45$ and 0.7, respectively, i.e., even negative total gluon polarizations are compatible with present data. The same results hold of course also in LO. Future dedicated polarized small-x measurements and upcoming determinations of $\delta g(x,Q^2)$ should be useful in removing such extrapolation ambiguities caused by our present poor knowledge of $\delta g(x,Q^2)$.

Our corresponding LO and NLO parton distributions at the respective input scales $Q^2 = \mu_{LO,NLO}^2$ in Eq. (2.6) with the standard scenario fit parameters given in Table I are shown in Fig. 4. The main differences between our new input densities and our old GRSV95 ones [1] are somewhat harder δd (due to the new neutron data) and δg distributions although, as discussed above, the polarized gluon distribution in Fig. 4 is only slightly preferred by our ''optimal'' fit to presently available data. The polarized input densities in Figs. 4(a) and 4(b) are compared with our reference unpolarized valence-like LO and NLO dynamical input densities of Ref. [25] which satisfy, of course, the positivity requirement $|\delta f| \leq f$ as is obvious from Eq. (2.6). It should be nevertheless emphasized that the parameters, resulting from our rather general LO and NLO fits, are always such that these positivity conditions are automatically satisfied, i.e., there is practically no need to impose them separately. The distributions at $Q^2 = 5$ GeV^2, as obtained from these LO and NLO inputs at $Q^2 = \mu^2$, are shown in Fig. 5 where they are also compared with our old NLO GRSV95 [1] results. It should be noted that the substantially harder input polarized gluon density $x\delta g(x,\mu^2)$, in particular in LO, in Fig. 4(a) as compared to our old GRSV 95 fit, causes the sea density $x\delta\bar{q}(x,Q^2)$ to oscillate (slightly) in the large-x region at $Q^2 > \mu^2$ as shown in Fig. 5 [38].
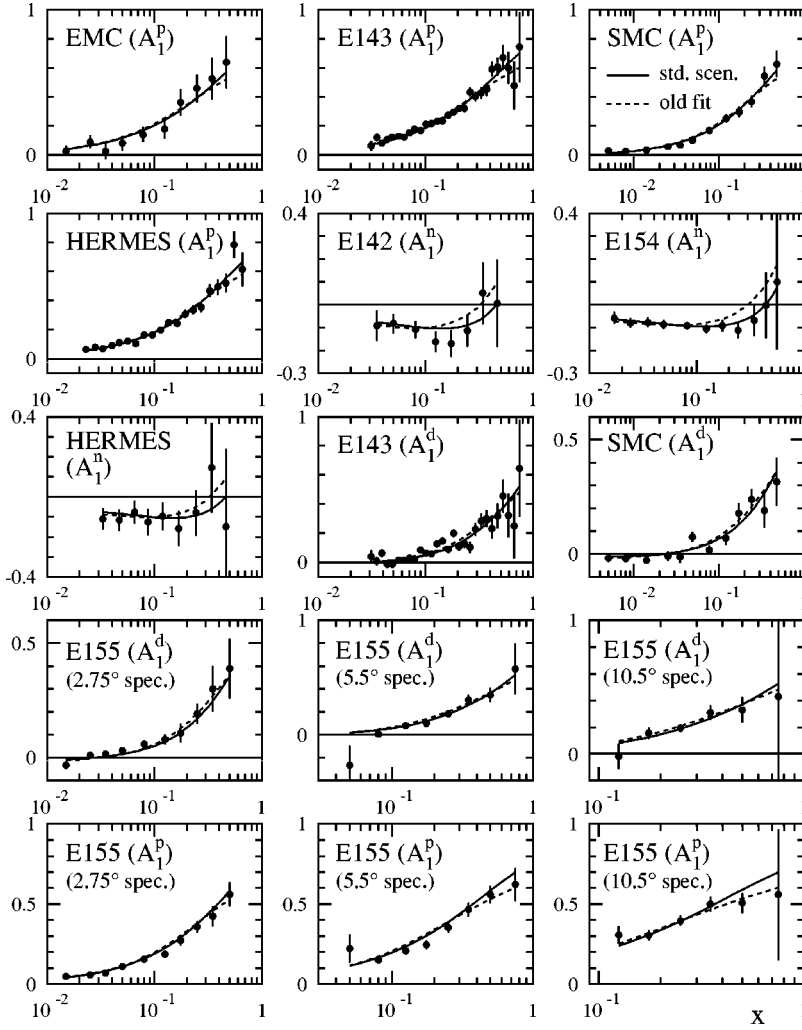
FIG. 1. Comparison of our NLO results for $A_1^N(x,Q^2)$ as obtained from the fitted input at $Q^2=\mu_{\mathrm{NLO}}^2$ for the standard $SU(3)_f$ flavor-symmetric sea scenario [Eq. (2.6) and Table I] with present data [16–24]. The Q^2 values adopted here correspond to the different values quoted in Refs. [16–24] for each data point starting at $Q^2 \gtrsim 1$ GeV^2 at the lowest available x bin. Our old NLO GRSV95 fit [1] is shown for comparison as well (dashed curves). Our present LO fit is very similar to the NLO one shown by the solid curves.

Next let us turn to the first moments (total polarizations) $\Delta f(Q^2)$ of our polarized parton distributions, as defined in Eq. (1.3), and the resulting $\Gamma_1^{p,n}(Q^2)$ in Eq. (1.5). It should be recalled that, in contrast to the LO, the first moments of the NLO (anti)quark densities do renormalize in the $\overline{\mathrm{MS}}$ scheme, i.e., are Q^2 dependent (see, e.g., Ref. [1]), whereas the gluon polarization $\Delta g(Q^2)$ renormalizes in both cases. Our LO standard fit implies

$$\Delta u = 0.871, \ \Delta d = -0.396, \ \Delta\bar{q} = \Delta s = \Delta\bar{s} = -0.054,$$

$$\Delta g(\mu_{\mathrm{LO}}^2) = 0.190, \ \Delta g(5 \text{ GeV}^2) = 0.684,$$

$$\Delta g(10 \text{ GeV}^2) = 0.802, \tag{2.7}$$

which result in $\Delta\Sigma = 0.259$ and

$$\Gamma_1^p = 0.151, \ \Gamma_1^n = -0.061. \tag{2.8}$$

Our NLO results are summarized in Table II at some typical values of Q^2. Both our LO and NLO results for $\Gamma_1^{p,n}(Q^2)$ are in satisfactory agreement with recent experimental determinations [17–24]. Furthermore, due to the constraint (2.1), the Bjorken sum rule [39] holds manifestly in LO and, according to Eq. (1.5), the NLO α_s-corrected sum rule reads

$$\Gamma_1^p(Q^2) - \Gamma_1^n(Q^2) = \frac{1}{6} g_A \left(1 - \frac{\alpha_s(Q^2)}{\pi} \right). \tag{2.9}$$

It is also interesting to observe that at our low input scales $Q^2 = \mu_{\mathrm{LO,NLO}}^2 = 0.26, 0.40 \text{ GeV}^2$ the nucleon's spin carried by the total helicities of quarks and gluons amounts only to

$$\frac{1}{2}\Delta\Sigma + \Delta g(\mu_{\mathrm{LO}}^2) \simeq 0.32,$$

$$\frac{1}{2}\Delta\Sigma(\mu_{\mathrm{NLO}}^2) + \Delta g(\mu_{\mathrm{NLO}}^2) \simeq 0.35, \tag{2.10}$$

which implies for the helicity sum rule (1.9) already a sizeable orbital contribution $L_{q+g}(\mu_{\mathrm{LO,NLO}}^2) \simeq 0.18, 0.15$ at the low input scales. Although this is in contrast to our somewhat more intuitive previous GRSV95 result [1], $L_{q+g}(\mu_{\mathrm{LO,NLO}}^2) \simeq 0$, it should be kept in mind that, for the time being, $\Delta g(Q^2)$ is rather weakly constrained by present data as was discussed above.

Finally, for completeness we have also performed a NLO analysis in a different factorization scheme, the so-called chirally invariant (CI) or JET scheme [8,40,41], but any other choice would do as well for studying the scheme de-
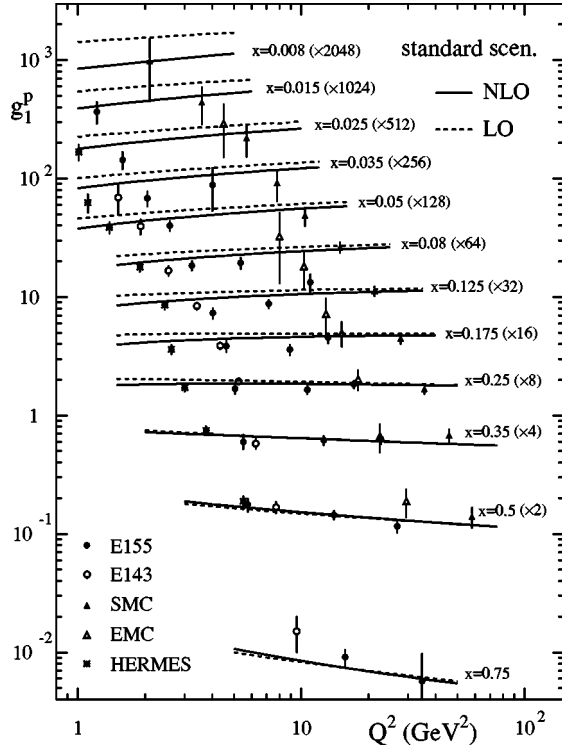
FIG. 2. Comparing the Q^2 dependence of our LO and NLO standard scenario results with recent data [16–18,21,24] on $g_1^p(x,Q^2)$. To ease the graphical representation we have multiplied all results at the various fixed values of x by the numbers indicated in parentheses.

FIG. 3. The x dependence of g_1^N at $Q^2 = 5$ GeV^2 in the NLO standard scenario. Different choices of the gluon input $\delta g(x,\mu^2_{\rm NLO})$ in Eq. (2.6) are shown by the dashed and dotted curves as indicated. Allowing our optimal total χ^2 to change by one unit, $\delta\chi^2 = \pm 1$, results in the shaded areas shown. The data are taken from Refs. [17], [18], [20], and [22–24].

pendence of our $\overline{\rm MS}$ fit results. Here, among other things [8,40,41], the total helicity of quarks, $\Delta\Sigma_{\rm CI}$, is conserved, i.e., Q^2 independent, and is related to our $\Delta\Sigma$ in the $\overline{\rm MS}$ scheme via

$$\Delta\Sigma(Q^2) = \Delta\Sigma_{\rm CI} - 3\frac{\alpha_s(Q^2)}{2\pi}\Delta g(Q^2)_{\rm CI}. \quad (2.11)$$

Similarly agreeable fits as the ones in Figs. 1–3 can be obtained in this scheme, e.g., by choosing a large positive gluon density with a total (input) helicity $\Delta g(\mu^2_{\rm NLO})_{\rm CI} \simeq 0.6\text{–}0.7$ being about three times larger than in Table II and the sea density $\delta\bar{q}_{\rm CI}(\Delta\bar{q}_{\rm CI})$ turns out to be roughly 50% smaller than the one of our best fit in the $\overline{\rm MS}$ standard scenario; here the total quark helicity increases to $\Delta\Sigma_{\rm CI}\simeq 0.4$.

III. $SU(3)_f$ BROKEN "VALENCE" (BROKEN-SEA) SCENARIO

The assumption of the flavor symmetric standard scenario with its unbroken sea density in Eq. (2.5) is expected to be unrealistic, following our experience in the unpolarized case where a suppression of the strange sea component is required, as accomplished by the vanishing input $s(x,\mu^2) = \bar{s}(x,\mu^2) = 0$ in GRV98 [25], in order to comply with experimental indications [42,43] of an $SU(3)_f$ broken sea, and the positivity constraint $\delta s \lesssim s$. Thus in GRSV95 [1] we also considered a valence scenario where, in contrast to Eq. (2.5),
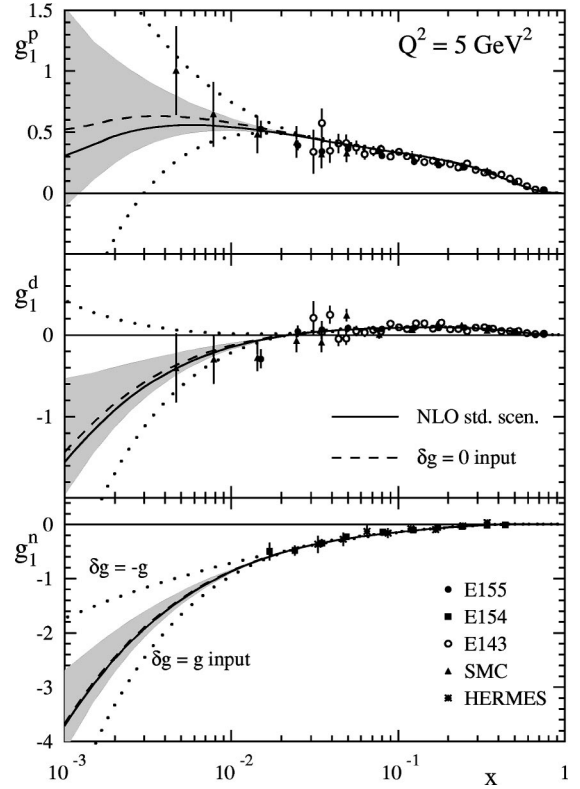
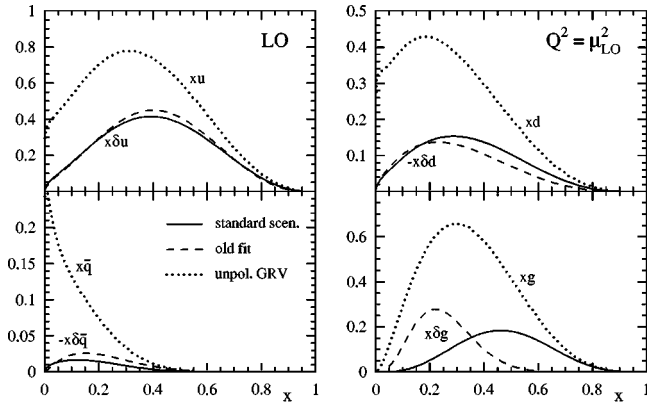$$\delta\bar{q}(x,\mu^2) \equiv \delta\bar{u} = \delta\bar{d} = \delta u_{\rm sea} = \delta d_{\rm sea},$$

$$\delta s(x,\mu^2) = \delta\bar{s}(x,\mu^2) = 0. \quad (3.1)$$

Furthermore, the full $SU(3)_f$ flavor symmetry, giving rise to the constraints (2.1) and (2.2), is broken in the valence scenario to the extent [44] that the flavor-changing hyperon β-decay data fix *only* the total helicity of *valence* quarks $\Delta q_v \equiv \Delta q - \Delta\bar{q}$:
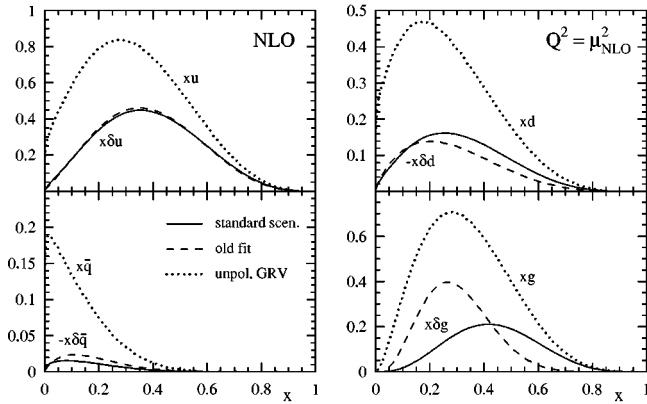
$$\Delta u_v(\mu^2) - \Delta d_v(\mu^2) = F + D \quad (3.2)$$

$$\Delta u_v(\mu^2) + \Delta d_v(\mu^2) = 3F - D, \quad (3.3)$$

i.e., $\Delta q_3 = \Delta u_v - \Delta d_v$ and $\Delta q_8 = 3F - D + 4\Delta\bar{q}$ at $Q^2 = \mu^2$ [1] according to Eq. (3.1). Therefore a light polarized sea $\Delta\bar{q} < 0$ suffices here to account for the reduction of the Ellis-Jaffe estimate (2.4). This is the reason for our simplifying assumption of a maximally broken $SU(3)_f$ strange sea input in Eq. (3.1) in order to reduce the number of input distributions to be fitted to the rather scarce available polarization data, which are now sufficient for fixing these input distributions. [Future high-statistics data should allow us, at least in principle, to extract the total strange sea polarization without employing any simplifying assumption, as, for example, from Eq. (1.8), $\Delta(s+\bar{s}) = (\Delta\Sigma - \Delta q_8)/3$]. The quality of the

FIG. 5. The polarized LO and NLO($\overline{\text{MS}}$) distributions at $Q^2 = 5$ GeV^2 in the standard scenario, as obtained from the input densities at $Q^2 = \mu^2_{\text{LO,NLO}}$ in Fig. 4. Our old NLO results [1] are shown for comparison.

FIG. 4. (a) Comparison of our fitted standard LO input distributions in Eq. (2.6) and Table I at $\mu^2_{\text{LO}} = 0.26$ GeV^2 with our previous old GRSV95 fit [1] and with the unpolarized dynamical GRV98 input densities of Ref. [25]. (b) The same as in (a) but for the NLO input densities at $\mu^2_{\text{NLO}} = 0.40$ GeV^2.

fits obtained is comparable to that of the standard flavor-symmetric scenario discussed and presented in the previous section, cf. Fig. 1. We refrain, however, from presenting these results here explicitly because the assumed remaining flavor-isospin symmetry of the light sea components in Eq. (3.1) appears to be somewhat artificial and unnatural in view of the flavor-asymmetric unpolarized light sea distributions $\bar{d}(x,Q^2) > \bar{u}(x,Q^2)$ [25–28].

Turning now to the presumably more realistic scenario where also the *flavor-isospin symmetry of the polarized sea is broken*, we note, as already pointed out in the Introduction,
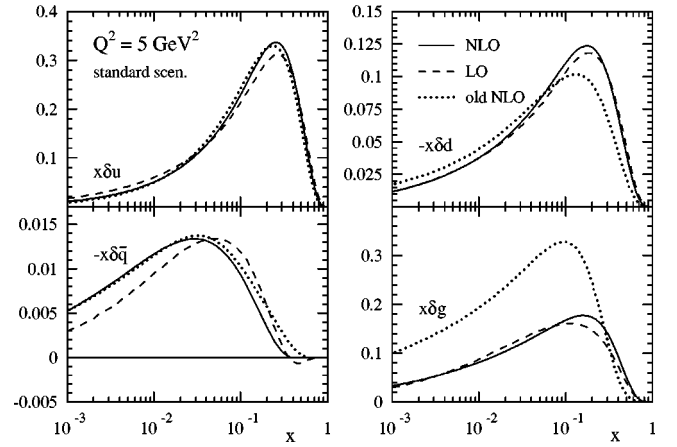
that some model assumptions are needed for the corresponding input distributions. The analysis of the unpolarized structure functions yields

$$\bar{d}(x,\mu^2)/\bar{u}(x,\mu^2) \simeq u(x,\mu^2)/d(x,\mu^2), \qquad (3.4)$$

which holds to a rather good accuracy for the GRV98 distributions [25]. This proportionality relation is expected to hold approximately at least for $0.01 \lesssim x \lesssim 0.3$ where the breaking of the light sea $\bar{d} > \bar{u}$ is directly tested experimentally via Drell-Yan dilepton production in pp and pd collisions [45] and semi-inclusive $\pi^{\pm}$ production in ep and ed reactions [46]. The relation (3.4) may be considered [30] as a manifestation of the Pauli-blocking effect [47] which should be relevant also in the polarized parton sector. We therefore estimate the flavor-symmetry breaking of the polarized sea to be given in a first approximation by [30]

$$\delta\bar{d}(x,\mu^2)/\delta\bar{u}(x,\mu^2) = \delta u(x,\mu^2)/\delta d(x,\mu^2) \qquad (3.5)$$

together with the previously advocated

$$\delta s(x,\mu^2) = \delta\bar{s}(x,\mu^2) = 0. \qquad (3.6)$$

According to the unpolarized case above, we expect the proportionality relation (3.5) to hold approximately at least for $0.01 \lesssim x \lesssim 0.3$.

TABLE II. First moments (total polarizations) Δf of polarized NLO parton densities $\delta f(x,Q^2)$ and $g_1^{p,n}(x,Q^2)$, defined in Eqs. (1.3) and (1.4), as obtained in the standard scenario. The marginal differences between $\Delta\bar{u}$ and $\Delta\bar{d}$ at $Q^2 > \mu^2$, generated dynamically by the NLO evolution, are not displayed.

Q^2 (GeV^2)	Δu	Δd	$\Delta\bar{q}$	Δg	$\Delta\Sigma$	Γ_1^p	Γ_1^n
μ^2_{NLO}	0.863	-0.404	-0.062	0.240	0.211	0.119	-0.054
1	0.861	-0.405	-0.063	0.420	0.204	0.127	-0.058
5	0.859	-0.406	-0.064	0.708	0.197	0.132	-0.062
10	0.859	-0.406	-0.064	0.828	0.197	0.133	-0.063

It should be re-emphasized that, in complete analogy to unpolarized DIS, data on inclusive polarized DIS in kinematical regimes where only photon exchange is relevant give information only on the sums of quark and antiquark polarizations for each flavor, $\delta q(x,Q^2) + \delta \bar{q}(x,Q^2)$, appearing in $g_1(x,Q^2)$ in Eq. (1.2). This implies, in particular, that the amount of flavor-SU(2) breaking in the polarized sea cannot be determined from such data since one can always change the parton densities by $\delta q \rightarrow \delta q - \delta \phi_q$ and $\delta \bar{q} \rightarrow \delta \bar{q} + \delta \phi_q$ for any arbitrary functions $\delta \phi_u(x)$ and $\delta \phi_d(x)$ *without* affecting at all the measured structure functions $g_1^{p,n,d}(x,Q^2)$. Restrictions on $\delta \phi_q(x)$ occur only in our valence scenario where $\Delta \phi_d = -\Delta \phi_u$ for the first moments, as in general implied by our modified ($\Delta \bar{u} \neq \Delta \bar{d}$) valence scenario constraints (3.7) and (3.8) below, and which have to even vanish for the ''unbroken'' ($\Delta \bar{u} = \Delta \bar{d}$) constraints (3.2) and (3.3). Therefore, for the time being, one has to resort to some, as far as possible, general and not too restrictive model assumptions concerning the breaking of the flavor- symmetry of the polarized light sea ($\delta \bar{u} \neq \delta \bar{d}$), such as the proportionality (3.5). Only future polarized $\vec{p}\vec{p}$ and $\vec{p}\vec{d}$ Drell-Yan $\mu^+ \mu^-$ pair and weak vector boson production experiments [48] as well as polarized semi-inclusive DIS $\vec{e}\vec{p}(d) \rightarrow e(\pi,K)X$ experiments [49,50] can provide us with direct measurements of the individual $\delta \bar{u}(x,Q^2)$ and $\delta \bar{d}(x,Q^2)$ distributions.

We now have, instead of Eq. (3.2),

$$\Delta q_3 = \Delta u_v(\mu^2) - \Delta d_v(\mu^2) + 2[\Delta \bar{u}(\mu^2) - \Delta \bar{d}(\mu^2)] = F + D,$$
$$(3.7)$$

and on account of Eqs. (3.3) and (3.6)

$$\Delta q_8(\mu^2) = \Delta u_v(\mu^2) + \Delta d_v(\mu^2) + 2[\Delta \bar{u}(\mu^2) + \Delta \bar{d}(\mu^2)],$$

$$= 3F - D + 2[\Delta \bar{u}(\mu^2) + \Delta \bar{d}(\mu^2)],$$

$$= \Delta \Sigma(\mu^2), \qquad (3.8)$$

where the imposed constraint (3.7) guarantees that the Bjorken sum rule (2.9) holds manifestly. Thus Eq. (1.5) becomes

$$\Gamma_1^{p,n}(Q^2) = \left[\pm \frac{1}{12}(F+D) + \frac{5}{36}(3F-D) + \frac{10}{36}[\Delta \bar{u}(Q^2) + \Delta \bar{d}(Q^2)] \right] \left(1 - \frac{\alpha_s(Q^2)}{\pi} \right) \qquad (3.9)$$

apart from a marginal contribution $\Delta s(Q^2) = \Delta \bar{s}(Q^2) < 0$ which is generated dynamically via the NLO evolution to $Q^2 > \mu_{\mathrm{NLO}}^2$ even for the vanishing input in Eq. (3.6). Thus, in this case, only the *total* light-quark sea contribution in Eq. (3.9) has to be *negative*, $\Delta \bar{u}(Q^2) + \Delta \bar{d}(Q^2) < 0$, in order to achieve the experimentally required reduction of the Ellis-Jaffe expectation (2.4).

Our resulting input distributions can be parametrized as in Eq. (2.6) where now, instead of the unbroken $\delta \bar{q}$ sea, we have a similar parametrization for $\delta \bar{u}(x,\mu^2)$ and $\delta \bar{d}(x,\mu^2)$

TABLE III. The parameters of the LO and NLO input distributions, as defined in Eq. (2.6), with $\bar{q}$ to be identified with $\bar{u}$, at $\mu_{\mathrm{LO}}^2 = 0.26$ GeV^2 and $\mu_{\mathrm{NLO}}^2 = 0.40$ GeV^2, respectively, for the valence scenario. We have fit the broken light-sea input density $\delta \bar{u}(x,\mu^2)$ and fixed $\delta \bar{d}(x,\mu^2)$ via Eqs. (3.5) and (3.4) [51].

| | Valence scenario | |
	LO	NLO
N_u	1.297	2.043
α_u	0.79	0.97
β_u	0.27	0.64
N_d	-2.496	-2.709
α_d	1.17	1.26
β_d	1.31	1.06
$N_{\bar{u}}$	2.005	1.727
$\alpha_{\bar{u}}$	0.79	0.73
$\beta_{\bar{u}}$	1.93	2.00
N_s	0	0
N_g	6.637	20.45
α_g	2.00	2.92
β_g	1.50	1.68
χ^2/209 data pts.	172.0	170.5

which are constrained by Eq. (3.5) [51], together with the respective flavor-broken unpolarized input densities $\bar{u}(x,\mu^2)$ and $\bar{d}(x,\mu^2)$ taken from Ref. [25]. The parameters of our optimal LO densities at $\mu_{\mathrm{LO}}^2 = 0.26 \, \mathrm{GeV}^2$ and the ones of the NLO($\overline{\mathrm{MS}}$) densities at $\mu_{\mathrm{NLO}}^2 = 0.40 \, \mathrm{GeV}^2$ are given in Table III. These optimal fits correspond to $\chi_{\mathrm{DF/LO}}^2 = 0.823$ and $\chi_{\mathrm{DF,NLO}}^2 = 0.816$ similarly to the standard scenario in Sec. II. The quality of these LO and NLO fits to $A_1^N(x,Q^2)$ in the broken valence scenario is practically identical to our new fit in the standard scenario shown in Fig. 1 by the solid curves. The same holds true also for $g_1^{p,n,d}(x,Q^2)$ shown in Figs. 2 and 3. The corresponding LO and NLO parton distributions at the respective input scales $Q^2 = \mu_{\mathrm{LO,NLO}}^2$ in Eq. (2.6) [51] with the valence scenario fit parameters given in Table III are shown in Fig. 6, which are also compared with our reference unpolarized valencelike dynamical input densities of Ref. [25] which satisfy the positivity constraint $|\delta f| \leq f$. The polarized gluon densities turn out to be somewhat larger here, in particular in NLO, than the ones in the standard scenario shown in Fig. 4. It should be furthermore emphasized that we always expect for the broken light-sea input densities to have a *positive* $\delta \bar{u}$ and a *negative* $\delta \bar{d}$ with $|\delta \bar{d}| > \delta \bar{u}$, i.e., $\delta \bar{u} - \delta \bar{d} > 0$ and $\delta \bar{u} + \delta \bar{d} < 0$.

In Fig. 7 we present the flavor asymmetry $x(\delta \bar{u} - \delta \bar{d})(x,\mu^2)$ separately, as obtained from Fig. 6, which compares favorably with predictions of the relativistic field theoretical chiral quark-soliton model [52,50]. Similar results have been obtained by a recent analysis [53] based on the statistical parton model which are supposed to hold at a
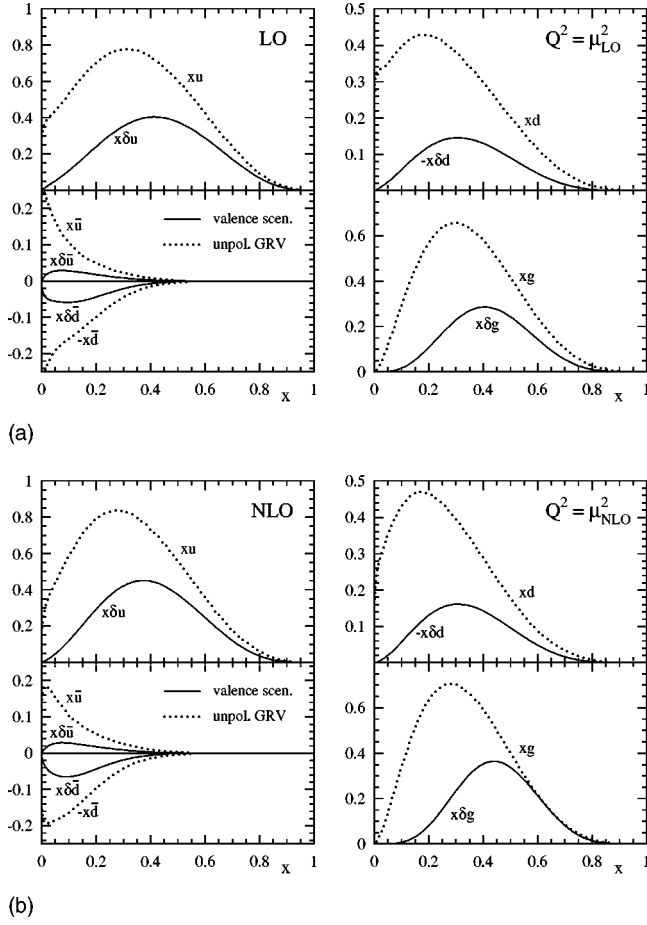
(a)

(b)

FIG. 6. (a) Comparison of our fitted fully broken valence scenario LO input distributions in Eq. (2.6) [51] and Table III at μ^2_{LO} $=0.26\,\text{GeV}^2$ with the unpolarized GRV98 input densities of Ref. [25]. (b) The same as in (a) but for the NLO input densities at $\mu^2_{NLO}=0.40\,\text{GeV}^2$.

somewhat larger input scale $Q^2_0=M^2_p\simeq0.9\,\text{GeV}^2$. We note furthermore that the prediction $\delta g(x,M^2_p)=0$ of this latter model is consistent with the results of the present analysis which do *not* exclude this possibility, cf. Fig. 3. The resulting NLO distributions at $Q^2=5\,\text{GeV}^2$ are shown in Fig. 8 where they are also compared with our new NLO results obtained in the standard scenario as shown by the solid curves in Fig. 5.

The first moments (total polarizations) $\Delta f(Q^2)$ of the polarized parton distributions of our fully flavor-broken valence scenario and the resulting $\Gamma^{p,n}_1(Q^2)$ are in LO given by

$$\Delta u=0.664,\ \ \Delta d=-0.248,\ \ \Delta\bar{u}=0.093,$$

$$\Delta\bar{d}=-0.261,\ \ \Delta s=\Delta\bar{s}=0,$$

$$\Delta g(\mu^2_{LO})=0.300,\ \ \Delta g(5\,\text{GeV}^2)=0.963,$$

$$\Delta g(10\,\text{GeV}^2)=1.122 \qquad (3.10)$$

which result in $\Delta\Sigma=0.248$ and

$$\Gamma^p_1=0.140,\ \ \Gamma^n_1=-0.071. \qquad (3.11)$$

Our NLO results are summarized in Table IV at some typical values of Q^2. The nucleon's spin is carried almost entirely by the total helicities of quarks and gluons at the LO and NLO input scales

$$\frac{1}{2}\Delta\Sigma(\mu^2_{LO,NLO})+\Delta g(\mu^2_{LO,NLO})\simeq0.42,\ \ 0.48 \quad (3.12)$$

which is larger than the standard scenario results (2.10), and thus a very small orbital contribution $L_{q+g}(\mu^2_{LO,NLO})$ $\simeq0.08,0.02$ is required at the low input scales in order to comply with the sum rule (1.9). This is somewhat similar to our previous results [1], but again $\Delta g(Q^2)$ is not strongly constrained by present data. Nevertheless it is intuitively appealing that this nonperturbative orbital (angular momentum) contribution to the helicity sum rule (1.9) vanishes at our low input scales, $L_{q+g}(\mu^2)\simeq0$. This is in contrast to larger scales $Q^2>\mu^2$ where hard radiative effects give rise to sizeable orbital components due to the increasing k_T of the partons, which eventually have to compensate in Eq. (1.9) the strongly increasing gluon polarization $\Delta g(Q^2)\sim\alpha^{-1}_s(Q^2)$: in both scenarios we obtain, for example, $\Delta g(10\ \text{GeV}^2)$ $\simeq1$.

Finally let us conclude with a few remarks concerning the flavor-symmetry breaking which was implemented in our broken valence scenario via the entirely empirical relation (3.5). On rather general grounds one expects the product

$$\delta q(x,\mu^2)\,\delta\bar{q}(x,\mu^2)\equiv P(x) \qquad (3.13)$$

to be a universal flavor-*independent* function $P(x)$, since the effect of Pauli blocking is only related to the spin (helicities) of quarks and antiquarks irrespective of their flavor degree of freedom. This implies $\delta u(x,\mu^2)\,\delta\bar{u}(x,\mu^2)$ $=\delta d(x,\mu^2)\,\delta\bar{d}(x,\mu^2)$, i.e., Eq. (3.5). Furthermore, we have seen that the data select, within our valence scenario with its
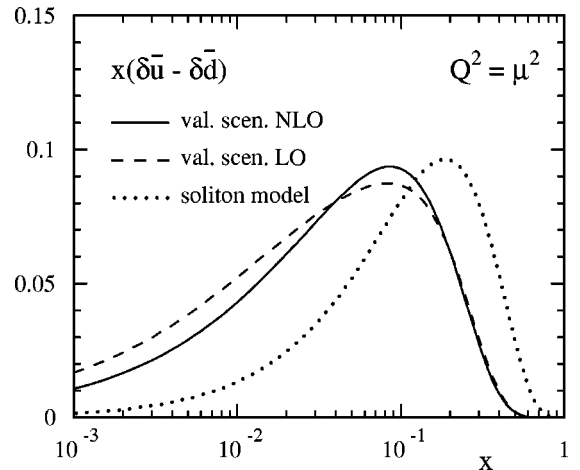

FIG. 7. LO and NLO results for the difference of the broken light-sea input densities $\delta\bar{u}(x,\mu^2)$ and $\delta\bar{d}(x,\mu^2)$ in the valence scenario as obtained from Fig. 6. The prediction of the chiral quark-soliton model is taken from K. Goeke *et al.* [52].
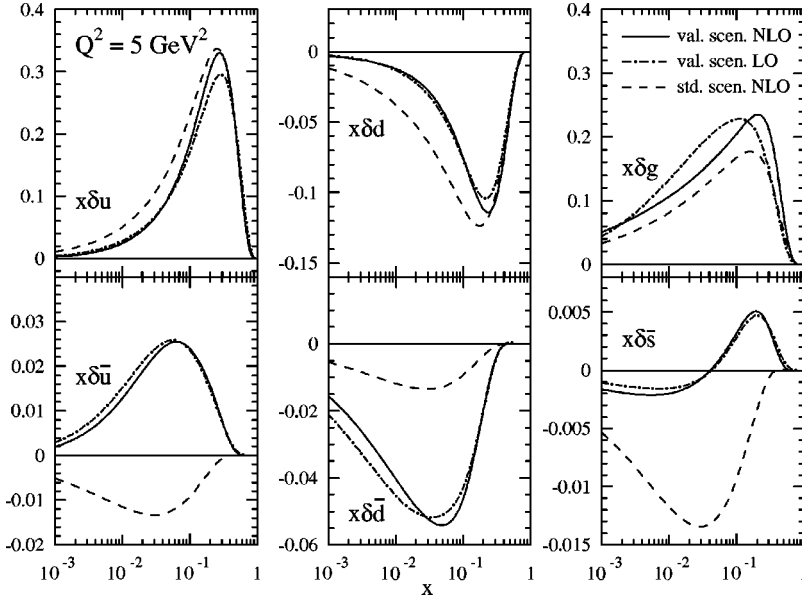
FIG. 8. The polarized LO and NLO($\overline{\text{MS}}$) distributions at $Q^2 = 5 \text{ GeV}^2$ in the fully flavor-broken valence scenario, as obtained from the input densities at $Q^2 = \mu^2_{\text{LO,NLO}}$ in Fig. 6. For comparison the new NLO results of the standard (unbroken sea) scenario are shown as well by the dashed curves (which coincide with the solid curves of Fig. 5).

totally flavor-broken polarized light sea densities in Eqs. (3.5) and (3.6), the solution of Eq. (3.5) which satisfies $P(x) > 0$ in Eq. (3.13) for $q = u, d$ as can be seen in Fig. 6. This can be understood [30] as a consequence of the expected predominant *pseudoscalar* configuration [29,54] of the quark-antiquark pairs in the nucleon sea. In fact, the two relations $u\bar{u} \simeq d\bar{d}$ and $\delta u \delta \bar{u} = \delta d \delta \bar{d}$ at the input scale $Q^2 = \mu^2$ can be rewritten as

$$P_p(x) \equiv u_+ \bar{u}_+ + u_- \bar{u}_- \simeq d_+ \bar{d}_+ + d_- \bar{d}_- ,$$

$$P_a(x) \equiv u_+ \bar{u}_- + u_- \bar{u}_+ \simeq d_+ \bar{d}_- + d_- \bar{d}_+ \qquad (3.14)$$

with $P = P_p - P_a$ in Eq. (3.13) and the common helicity densities being given by $\overset{(-)}{q}_{\pm} = (\overset{(-)}{q} \pm \delta \overset{(-)}{q})/2$ where for brevity we have dropped the x dependence. A predominant pseudoscalar configuration of $(q\bar{q})$ pairs in the nucleon sea implies, via Pauli blocking, that the aligned quark-quark configurations $q_+(q_+\bar{q}_-)$ and $q_-(q_-\bar{q}_+)$ are suppressed relatively to the antialigned $q_+(q_-\bar{q}_+)$ and $q_-(q_+\bar{q}_-)$ "cloud" configurations, i.e., $P_p(x) > P_a(x)$ which implies $P(x) > 0$ in Eq. (3.13). The result for P_p/P_a, corresponding to our optimal fit, is shown in Fig. 9: clearly, this ratio will be maximal where $xq(x,\mu^2)$ and $x\delta q(x,\mu^2)$ are maximal at $x \simeq 0.2$–0.4, cf. Fig. 6, i.e., where the Pauli blocking, Eq. (3.13), is most effective which is nicely exhibited in Fig. 9 in LO and NLO.

It is interesting to mention that some of these expectations, which derive mainly from our light-sea flavor breaking relation (3.5), have been already confirmed by a recent entirely independent simultaneous analysis [14] of polarized DIS and semi-inclusive deep inelastic scattering (SIDIS) asymmetry data. In particular the more recent high precision SIDIS HERA-HERMES data [55] on h^+ production ($h = \pi, K$ dominantly) off a proton target $\vec{e}\vec{p} \to e h^+ X$, seem to play a decisive role in favoring flavor-broken light sea densities $\delta \bar{u}(x, Q^2) \neq \delta \bar{d}(x, Q^2)$, despite the fact that these asymmetry data on $A^{h^+}_{1p}$ refer to rather small scales $Q^2 \gtrsim 1 \text{ GeV}^2$. The reason for this discriminative power is, when combined with the data from inclusive DIS, due to the fact that $A^{h^+}_{1p}$ is proportional [14], besides to the dominant valence contribution, also to $\delta\bar{d} - 4\delta\bar{u}$, multiplied by a "favored" fragmentation function, which is significantly more sensitive to $\delta\bar{u}$ than to $\delta\bar{d}$. A clear preference for a *positive* $\delta\bar{u}$ has been observed [14], which is very similar to our NLO $\delta\bar{u}$ shown in Fig. 6(b), and a flavor symmetric standard light sea scenario seems to be strongly disfavored.

We have calculated at NLO the spin asymmetries for semi-inclusive DIS using the well-known theoretical SIDIS framework [56,14] together with our results for the polarized parton distributions of the standard and valence scenario with their flavor-symmetric and flavor-broken light sea densities, respectively, employing the fragmentation functions of

TABLE IV. First moments (total polarizations) Δf of polarized parton densities $\delta f(x, Q^2)$ and $g_1^{p,n}(x, Q^2)$, defined in Eqs. (1.3) and (1.4), as obtained in the fully flavor-broken valence scenario. The marginal finite $\Delta s = \Delta \bar{s}(Q^2 > \mu^2_{\text{NLO}})$ are generated dynamically by the NLO evolution.

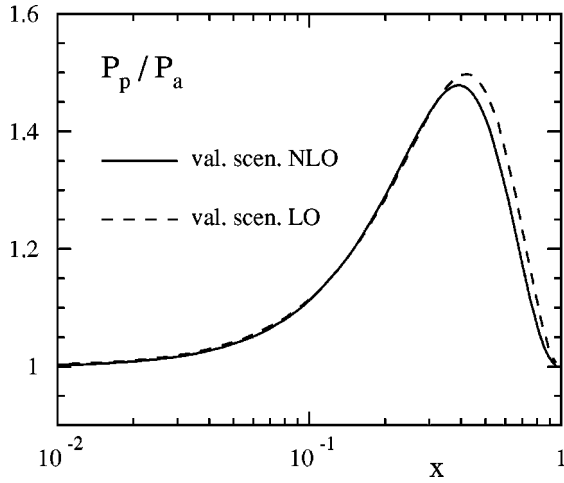| Q^2 (GeV^2)	Δu	Δd	$\Delta \bar{u}$	$\Delta \bar{d}$	$\Delta s = \Delta \bar{s}$	Δg	$\Delta \Sigma$	Γ_1^p	Γ_1^n
μ^2_{NLO}	0.693	-0.255	0.087	-0.232	0	0.330	0.293	0.119	-0.053
1	0.691	-0.257	0.086	-0.234	-1.95×10^{-3}	0.579	0.282	0.127	-0.058
5	0.689	-0.258	0.085	-0.235	-3.31×10^{-3}	0.974	0.273	0.132	-0.062
10	0.688	-0.258	0.085	-0.236	-3.64×10^{-3}	1.140	0.272	0.133	-0.062

FIG. 9. The ratio of $P_p(x)$ and $P_a(x)$, defined in Eq. (3.14), at the LO and NLO input scales $\mu^2_{\text{LO,NLO}}$ which demonstrates the Pauli blocking of the disfavored antiparallel $q_\pm \bar{q}_\mp$ configurations relative to the favored parallel $q_\pm \bar{q}_\pm$ configurations as discussed in the text.

FIG. 10. NLO predictions for the semi-inclusive DIS asymmetry $A^{h^+}_{1p}$ for h^+ production off a proton target within the valence and standard scenario. The HERMES data are taken from Ref. [55].

Ref. [57]. (We did not use the alternative set of recent fragmentation functions suggested in Ref. [58], since they refer to scales Q^2 larger than 2 GeV^2.) The results for the relevant SIDIS asymmetry $A^{h^+}_{1p}$ are shown in Fig. 10. Although the high precision HERMES data [55] seem to favor slightly the valence scenario with its flavor-broken light sea, the results of the standard scenario with its flavor-symmetric light sea cannot yet be ruled out. Both scenarios in Fig. 10 give rise to a comparable $\chi^2/(9$ data points) of 7.6 and 8.5 for the valence and standard scenario, respectively.

IV. SUMMARY AND CONCLUSIONS

All recent polarized DIS data, including the most recent SLAC-E155 proton data [24], have been analyzed and studied within the standard and valence scenario in LO and NLO of QCD. The standard scenario, characterized by Eqs. (2.1) and (2.2), refers to the common simplified, but probably unrealistic, assumption of an SU(3)$_f$ flavor-symmetric polarized light sea. The original valence scenario [1], characterized by Eqs. (3.2) and (3.3), is now modified by employing a *totally* SU(3)$_f$ asymmetric polarized light sea $\delta \bar{u} \neq \delta \bar{d} \neq \delta \bar{s}$ which leads to the modified constraints (3.7) and (3.8). Since inclusive polarized DIS data cannot fix the flavor-broken sea densities, we have modeled the flavor-asymmetric light sea densities $\delta \bar{u} \neq \delta \bar{d}$ using a Pauli-blocking ansatz [30] in Eq. (3.5), because similar ''blocking'' effects can also explain the flavor asymmetry of unpolarized sea densities ($\bar{d} > \bar{u}$). All our resulting polarized parton distributions respect the fundamental positivity constraints down to the low resolution scales $Q^2 = \mu^2_{\text{LO}} = 0.26$ GeV^2 and $\mu^2_{\text{NLO}} = 0.40$ GeV^2. The polarized gluon distribution $\delta g(x, Q^2)$ is weakly constrained by present data in both scenarios. In particular, a vanishing

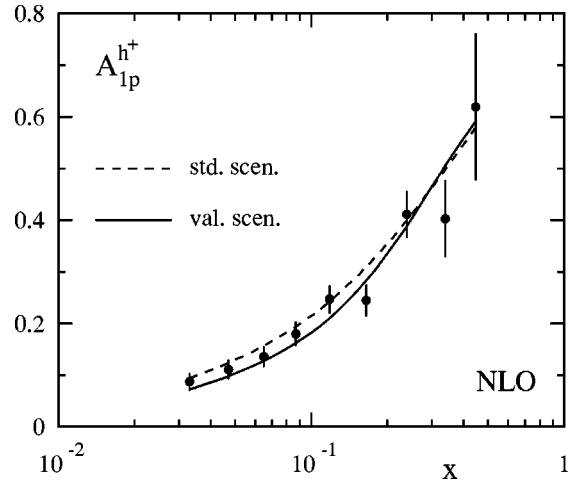gluon input $\delta g(x, \mu^2) = 0$ is equally compatible with all present measurements of $A^N_1(x, Q^2)$ or $g^N_1(x, Q^2)$. Only a fully saturated (via the positivity constraint) gluon input $\delta g(x, \mu^2) = \pm g(x, \mu^2)$ appears to be disfavored by present data.

The presumably more realistic valence scenario with its flavor-broken light sea quark distributions $\delta \bar{u} \neq \delta \bar{d} (\neq \delta \bar{s} = \delta s \simeq 0)$ leads to a *positive* $\delta \bar{u}(x, Q^2)$ density and a sizeably larger negative $\delta \bar{d}(x, Q^2)$. These results are supported by a recent combined analysis [14] of polarized DIS and semi-inclusive DIS data and agree with predictions of the relativistic field theoretical chiral quark-soliton model [52,50] and of the statistical parton model [53]. Present high statistics HERA-HERMES data [55] on semi-inclusive asymmetries $A^{h^\pm}_{1N}$ for $h^\pm$ production off nucleon targets cannot, however, yet uniquely discriminate between our valence scenario with flavor-broken polarized light sea densities and the common standard scenario with a flavor-symmetric light sea-quark distribution.

A FORTRAN package containing our optimally fitted standard and fully flavor-broken valence NLO($\overline{\text{MS}}$) as well as LO distributions can be obtained by electronic mail.

[1] M. Glück, E. Reya, M. Stratmann, and W. Vogelsang, Phys. Rev. D **53**, 4775 (1996).

[2] T. Gehrmann and W. J. Stirling, Phys. Rev. D **53**, 6100 (1996).

[3] R. D. Ball, S. Forte, and G. Ridolfi, Phys. Lett. B **378**, 255 (1996); G. Altarelli, R. D. Ball, S. Forte, and G. Ridolfi, Nucl. Phys. **B496**, 337 (1997); Acta Phys. Pol. B **29**, 1145 (1998).

[4] SLAC-E154 Collaboration, K. Abe *et al.*, Phys. Lett. B **405**, 180 (1997).

[5] CERN-SM Collaboration, B. Adeva *et al.*, Phys. Rev. D **58**, 112002 (1998).

[6] C. Bourrely, F. Buccella, O. Pisanti, P. Santorelli, and J. Soffer, Prog. Theor. Phys. **99**, 1017 (1998).

[7] D. de Florian, O. A. Sampayo, and R. Sassot, Phys. Rev. D **57**, 5803 (1998).

[8] E. A. Leader, A. V. Sidorov, and D. B. Stamenov, Int. J. Mod. Phys. A **13**, 5573 (1998); Phys. Rev. D **58**, 114028 (1998); Phys. Lett. B **445**, 232 (1998); **462**, 189 (1999); **488**, 283 (2000).

[9] L. E. Gordon, M. Goshtasbpour, and G. P. Ramsey, Phys. Rev. D **58**, 094017 (1998).

[10] SLAC-E154/155 Collaboration, S. Incerti and F. Sabatie, CEA-Saclay PCCF-RI-9901, 1999.

[11] S. Tatur, J. Bartelski, and M. Kurzela, Acta Phys. Pol. B **31**, 647 (2000); J. Bartelski and S. Tatur, hep-ph/0004251.

[12] D. K. Ghosh, S. Gupta, and D. Indumathi, Phys. Rev. D **62**, 094012 (2000).

[13] Asymmetry Analysis Collaboration, Y. Goto *et al.*, Phys. Rev. D **62**, 034017 (2000).

[14] D. de Florian and R. Sassot, Phys. Rev. D **62**, 094025 (2000).

[15] SLAC-Yale E80 Collaboration, M. J. Alguard *et al.*, Phys. Rev. Lett. **37**, 1261 (1976); G. Baum *et al.*, *ibid.* **45**, 2000 (1980); SLAC-Yale-E130 Collaboration, G. Baum *et al.*, *ibid.* **51**, 1135 (1983).

[16] CERN-EM Collaboration, J. Ashman *et al.*, Phys. Lett. B **206**, 364 (1988); Nucl. Phys. **B328**, 1 (1989).

[17] CERN-SM Collaboration, B. Adeva *et al.*, Phys. Rev. D **58**, 112001 (1998).

[18] SLAC-E143 Collaboration, K. Abe *et al.*, Phys. Rev. D **58**, 120003 (1998).

[19] SLAC-E142 Collaboration, P. L. Anthony *et al.*, Phys. Rev. D **54**, 6620 (1996).

[20] DESY-HERMES Collaboration, K. Ackerstaff *et al.*, Phys. Lett. B **404**, 383 (1997).

[21] DESY-HERMES Collaboration, A. Airapetian *et al.*, Phys. Lett. B **442**, 484 (1998).

[22] SLAC-E154 Collaboration, K. Abe *et al.*, Phys. Rev. Lett. **79**, 26 (1997).

[23] SLAC-E155 Collaboration, P. L. Anthony *et al.*, Phys. Lett. B **463**, 339 (1999).

[24] SLAC-E155 Collaboration, P. L. Anthony *et al.*, Phys. Lett. B **493**, 19 (2000).

[25] M. Glück, E. Reya, and A. Vogt, Eur. Phys. J. C **5**, 461 (1998).

[26] A. D. Martin, R. G. Roberts, W. J. Stirling, and R. S. Thorne, Eur. Phys. J. C **4**, 463 (1998); **14**, 133 (2000).

[27] CTEQ5 Collaboration, H. L. Lai *et al.*, Eur. Phys. J. C **12**, 375 (2000).

[28] H. Botje, Eur. Phys. J. C **14**, 285 (2000).

[29] For recent reviews see, for example, S. Kumano, Phys. Rep.

[303], 183 (1998); J. Speth and A. W. Thomas, Adv. Nucl. Phys. **24**, 83 (1998).

[30] M. Glück and E. Reya, Mod. Phys. Lett. A **15**, 883 (2000).

[31] W. Furmanski and R. Petronzio, Z. Phys. C **11**, 293 (1982).

[32] M. Glück, E. Reya, and W. Vogelsang, Nucl. Phys. **B351**, 579 (1991).

[33] Particle Data Group, C. Caso *et al.*, Eur. Phys. J. C **3**, 1 (1998).

[34] M. Karliner and H. J. Lipkin, Phys. Lett. B **461**, 280 (1999).

[35] J. Ellis and R. L. Jaffe, Phys. Rev. D **9**, 1444 (1974); **10**, 1669(E) (1974); M. Gourdin, Nucl. Phys. **B38**, 418 (1972).

[36] S. J. Brodsky and I. Schmidt, Phys. Lett. B **234**, 144 (1990); S. J. Brodsky, M. Burkardt, and I. Schmidt, Nucl. Phys. **B441**, 197 (1995); F. E. Close and D. Sivers, Phys. Rev. Lett. **39**, 1116 (1977).

[37] Note that our ansatz violates (slightly) the ''helicity retention'' concept developed in Ref. [36], by which $\delta f(x,Q^2)/f(x,Q^2) \to 1$ for $x \to 1$. Such relations follow in perturbative QCD and need not necessarily be fulfilled by our nonperturbative input at $Q^2 = \mu^2$. In any case, we could always appropriately modify our ansatz at very high x so as to satisfy the helicity retention conditions. Enforcing in our fits all β_f to vanish in Eq. (2.6) increases the total χ^2 by several units, giving rise to worse fits than our optimal ones.

[38] We have refrained from attempting to extract information from measurements of the spin asymmetry for photoproduction of oppositely charged hadron pairs presented by the HERMES collaboration [A. Airapetian *et al.*, Phys. Rev. Lett. **84**, 2584 (2000)]. Such data could in principle constrain the spin gluon density $\delta g(x,Q^2)$; however, the smallness of the hadron transverse momenta accessed in this experiment makes an interpretation of the data in terms of QCD hard scattering difficult. In fact, as stated by the HERMES collaboration, their published gluon asymmetry $\delta g(x,Q^2)/g(x,Q^2) = 0.41 \pm 0.18$ at $x \simeq 0.17$ and $Q^2 \equiv \langle p_T^2 \rangle = 2.1 \, \text{GeV}^2$, which implies $x \delta g(x,Q^2) \simeq 0.35 \pm 0.15$, actually compatible with our results in Fig. 5, does not include systematic theoretical errors. These could be sizeable in the low transverse momentum region considered.

[39] J. D. Bjorken, Phys. Rev. **148**, 1467 (1966); Phys. Rev. D **1**, 1376 (1970).

[40] H. Y. Cheng, Int. J. Mod. Phys. A **11**, 5109 (1996); Phys. Lett. B **427**, 371 (1998). The explicit transformation of the splitting functions (anomalous dimensions) and coefficient functions from the $\overline{\text{MS}}$ to the CI (JET) scheme can be found in this latter reference as well as in the third reference of Ref. [8].

[41] D. Müller and O. V. Teryaev, Phys. Rev. D **56**, 2607 (1997).

[42] CDHSW Collaboration, H. Abramowicz *et al.*, Z. Phys. C **15**, 19 (1982).

[43] CCFR Collaboration, C. Foudas *et al.*, Phys. Rev. Lett. **64**, 1207 (1990); S. A. Rabinowitz *et al.*, *ibid.* **70**, 134 (1993); A. O. Bazarko *et al.*, Z. Phys. C **65**, 189 (1995).

[44] H. J. Lipkin, Phys. Lett. B **256**, 284 (1991); **337**, 157 (1994); J. Lichtenstadt and H. J. Lipkin, *ibid.* **353**, 119 (1995).

[45] NA51 Collaboration, A. Baldit *et al.*, Phys. Lett. B **332**, 244 (1994); E866 Collaboration, E. A. Hawker *et al.*, Phys. Rev. Lett. **80**, 3715 (1998).

[46] HERMES Collaboration, C. A. Miller, Proceedings of DIS '99, Nucl. Phys. B (Proc. Suppl.) **79**, 146 (1999).

[47] R. D. Field and R. P. Feynman, Phys. Rev. D **15**, 2590 (1977).

[48] S. Kumano and M. Miyama, Phys. Lett. B **479**, 149 (2000); B. Dressler *et al.*, Univ. Bochum RUB-TPII-13/99, hep-ph/9910464; C. Bourrely and J. Soffer, Phys. Lett. B **314**, 132 (1993); Nucl. Phys. **B423**, 329 (1994).

[49] T. Morii and T. Yamanishi, Phys. Rev. D **61**, 057501 (2000).

[50] B. Dressler *et al.*, Eur. Phys. J. C **14**, 147 (2000).

[51] The easiest and most consistent way to implement directly (even for Mellin-n moments) the constraint (3.5) in a fit routine is to fit, for example, δu, δd, and $\delta \bar{u}$ according to the ansatz (2.6) which fix $\delta \bar{d}(x,\mu^2)$ via Eqs. (3.5) and (3.4): $\delta \bar{d}/\bar{d} \simeq (\delta u/u)(\delta \bar{u}/\bar{u})/(\delta d/d)$ where the unpolarized densities are taken from Ref. [25]. Thus $N_{\bar{d}} = N_u N_{\bar{u}}/N_d$, $\alpha_{\bar{d}} = \alpha_u + \alpha_{\bar{u}} - \alpha_d$, and $\beta_{\bar{d}} = \beta_u + \beta_{\bar{u}} - \beta_d$.

[52] D. Diakonov *et al.*, Nucl. Phys. **B480**, 341 (1996); Phys. Rev. D **56**, 4069 (1997); M. Wakamatsu and T. Kubota, *ibid.* **60**, 034020 (1999); K. Goeke *et al.*, Univ. Bochum RUB-TPII-18/99, hep-ph/0001272.

[53] R. S. Bhalerao, Phys. Lett. B **380**, 1 (1996); **387**, 881(E) (1996); talk given at the International Conference on QNP 2000, Adelaide, 2000, Nucl. Phys. **A680**, 62 (2000); R. S. Bhalerao, N. G. Kelkar, and B. Ram, Phys. Lett. B **476**, 285 (2000).

[54] N. N. Nikolaev *et al.*, Phys. Rev. D **60**, 014004 (1999).

[55] HERMES Collaboration, K. Ackerstaff *et al.*, Phys. Lett. B **464**, 123 (1999).

[56] D. de Florian, C. A. Garcia Canal, and R. Sassot, Nucl. Phys. **B470**, 195 (1996).

[57] S. Kretzer, Phys. Rev. D **62**, 054001 (2000).

[58] B. A. Kniehl, G. Kramer, and B. Pötter, Nucl. Phys. **B582**, 514 (2000).